Interference of Interchromophoric Energy-Transfer Pathways in π-Conjugated Macrocycles

Laura Alfonso Hernandez,[†] Tammie Nelson,[‡] Maxim F. Gelin,[¶] John M. Lupton,[§] Sergei Tretiak,*[,‡] and Sebastian Fernandez-Alberti*[,†]

[†]Universidad Nacional de Quilmes/CONICET, Roque Saenz Peña 352, B1876BXD Bernal, Argentina
[‡]Theoretical Division, Los Alamos National Laboratory, Los Alamos, New Mexico 87545, United States
[¶]Department of Chemistry, Technische Universität München, D-85747 Garching, Germany
[§]Institut für Angewandte und Experimentelle Physik, Universität Regensburg, Universitätsstrasse 31, 93053 Regensburg, Germany

Ⓢ *Supporting Information*

ABSTRACT: The interchromophoric energy-transfer pathways between weakly coupled units in a π-conjugated phenylene–ethynylene macrocycle and its half-ring analogue have been investigated using the nonadiabatic excited-state molecular dynamics approach. To track the flow of electronic transition density between macrocycle units, we formulate a transition density flux analysis adapted from the statistical minimum flow method previously developed to investigate vibrational energy flow. Following photoexcitation, transition density is primarily delocalized on two chromophore units and the system undergoes ultrafast energy transfer, creating a localized excited state on a single unit. In the macrocycle, distinct chromophore units donate transition density to a single acceptor unit but do not interchange transition density among each other. We find that energy transfer in the macrocycle is slower than in the corresponding half ring because of the presence of multiple interfering energy-transfer pathways. Simulation results are validated by modeling the fluorescence anisotropy decay.
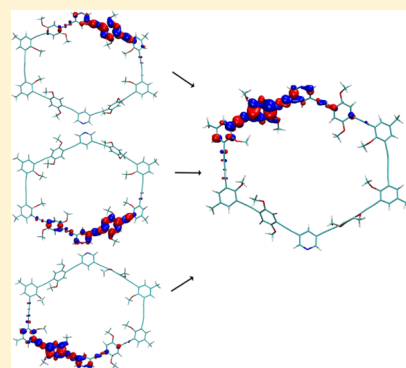
The complex interactions between π-conjugated organic polymers are responsible for phenomena ranging from morphology[1−3] and aggregation[4,5] in polymer films, rapid charge and energy transfer between coupled chromophores,[6−8] to the generation of charge-transfer excitons[9] and changes in absorption and emission[10] caused by strong interchain interactions. In natural light-harvesting complexes, both strong and weak interchromophoric dipole–dipole interactions exist simultaneously, and the interplay between these two interaction limits gives rise to the characteristically rich energy-transfer dynamics observed in these systems.[11−14]

It is well-known that exciton dynamics in π-conjugated molecular systems is highly susceptible to conformational disorder and electron–vibrational coupling. Thermally induced geometry distortions affect exciton localization and relaxation lifetimes and pathways, as reported in a large variety of extended conjugated molecular systems.[15−18] Ultrafast fluorescence depolarization measurements have confirmed that conformational disorder can lead to exciton self-trapping.[17] In fact, exciton localization during ultrafast energy transfer between chromophore units has been reported in cyclo-paraphenylene (CPP) and dimers.[7,19] Steric hindrance due to cyclic or curved polymer geometries introduces additional effects on the extent of conjugation.[20] In the particular case of nanorings, rapid formation of spatially localized excitations can occur as a consequence of the photoinduced self-trapping of the

lowest-energy excitonic state[19] due to strong electron–phonon coupling. To pinpoint the exact interchromophoric mechanisms at play in large complexes, model systems consisting of macrocyclic oligomers have been designed to serve as artificial light-harvesters, and their exciton localization and energy-transfer dynamics have been characterized.[21−28]

Despite these great efforts, a complete understanding of the energy-transfer dynamics, even in simplified model cyclic systems, remains elusive. For example, Lupton and co-workers[22] have studied the excited-state relaxation dynamics and concomitant interchromophoric energy transfer in π-conjugated phenylene–ethynylene macrocycles and their half-ring counterparts using fluorescence depolarization to detect changes in polarization caused by an excitation moving from one chromophore to another. It was concluded that the half ring does not appear to exhibit intramolecular energy transfer, whereas the macrocycles show an additional depolarization mechanism thought to arise from rapid redistribution of excitation energy occurring faster than 50 ps. This would suggest incoherent energy transfer between the chromophores in the macrocycle, consistent with the weak dipole–dipole coupling limit, where each chromophore behaves as a distinct
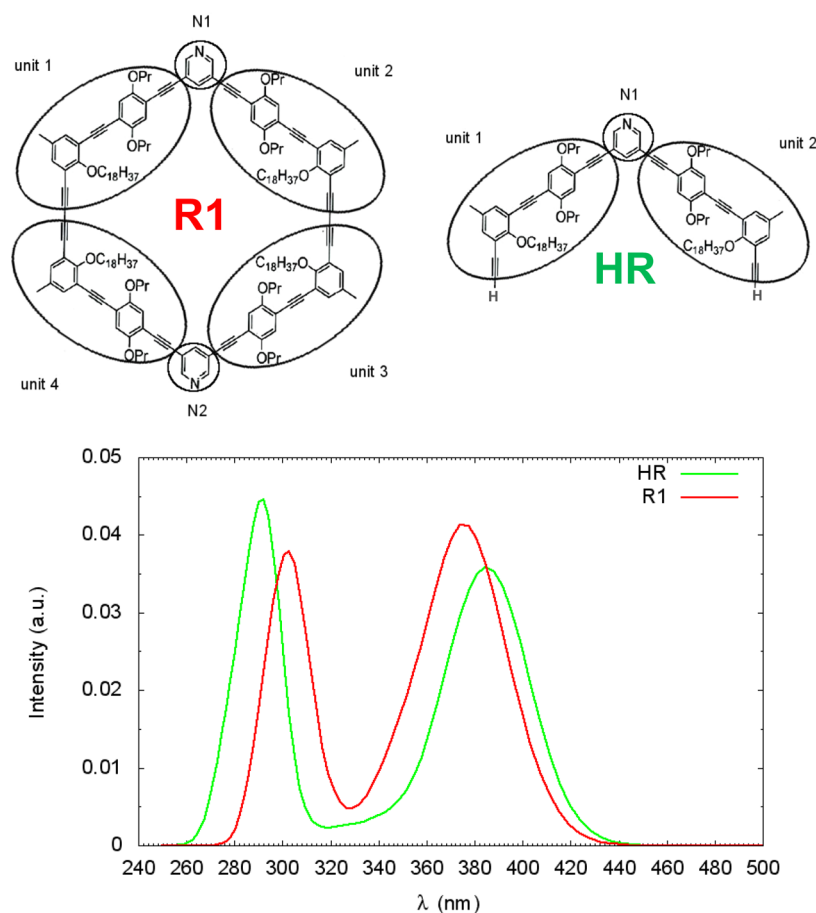
Figure 1. Chemical structures of macrocycle R1 and half ring HR showing selection of units and computed linear absorption spectra of R1 (red) and HR (green). For each geometry, the CEO method was used to compute the oscillator strengths and energies of excited states. The absorption spectra were computed by constructing histograms of the excited-state energies where the height is given by the average ratio between oscillator strength and frequencies.[58] Excitation energy for NA-ESMD simulations was chosen to correspond to the absorption maximum of the lowest-energy peak of the computed spectra, giving excitation wavelengths of 373 nm for R1 and 384 nm for HR.

unit. It is also conceivable that coherent coupling could occur between the chromophores; however, this is impossible to deduce directly from incoherent measurements of polarization anisotropy.

More recently, Herz and co-workers[28] have investigated the relationship between exciton delocalization dynamics and molecular size and topology in linear and cyclic porphyrin complexes. It was found that, for very large rings, absorbing and emitting states become localized, leading to similar overall anisotropy in both cyclic and linear geometries. Nevertheless, the stronger curvature enforced in cyclic structures leads to persistent faster anisotropy decay in rings compared to linear chains, even in large rings. This effect is expected to be amplified in smaller rings, which support delocalized absorbing ($S_0 \rightarrow S_2$) states but not delocalized emitting states ($S_1 \rightarrow S_0$). In such a case, rapid spatial localization of excitation energy could lead to spontaneous symmetry breaking, enabling fluorescence.[19,25,28−30]

In this respect, computational simulations can shed new light on the details of the underlying energy-transfer mechanisms. Such simulations can be performed using nonadiabatic excited-state molecular dynamics (NA-ESMD)[31,32] based on the fewest switches surface hopping (FSSH) approach[33] to go beyond the Born−Oppenheimer approximation and include coupling between many electronic excited states. These simulations can not only provide new insights into the evolution of the

electronic wave function and changes in exciton localization during nonradiative relaxation but also allow the fluorescence anisotropy signal to be directly modeled.[5]

Here, we use the NA-ESMD simulations to investigate the room-temperature (300 K) photoinduced energy-transfer dynamics between the chromophore units in a model π-conjugated phenylene−ethynylene macrocycle, R1, and the corresponding half-ring structure, HR, both of which have been previously examined spectroscopically.[22] Interchromophoric energy transfer is monitored in our simulations by tracking changes in electronic transition density (TD) localization. The specific energy flow between units is followed using transition density flux analysis according to the statistical minimum flow (SMF) method previously used to study the vibrational energy flow in polyatomic molecules.[34] The SMF adaptation for the transition density flux analysis is described in the Computational Methods section. Fluorescence anisotropy decay signals are also computed in order to understand the origin of fluorescence depolarization in the macrocycle configuration.

Both R1 and HR are composed of identical linear phenylene−ethynylene units identified in Figure 1. The structure of R1 is composed of four units with pyridine linking the two halves of the ring. The half-ring structure is identical to R1 but contains only two units. The computed absorption spectra, shown in the bottom panel of Figure 1, are in good agreement with experimentally measured solution-phase
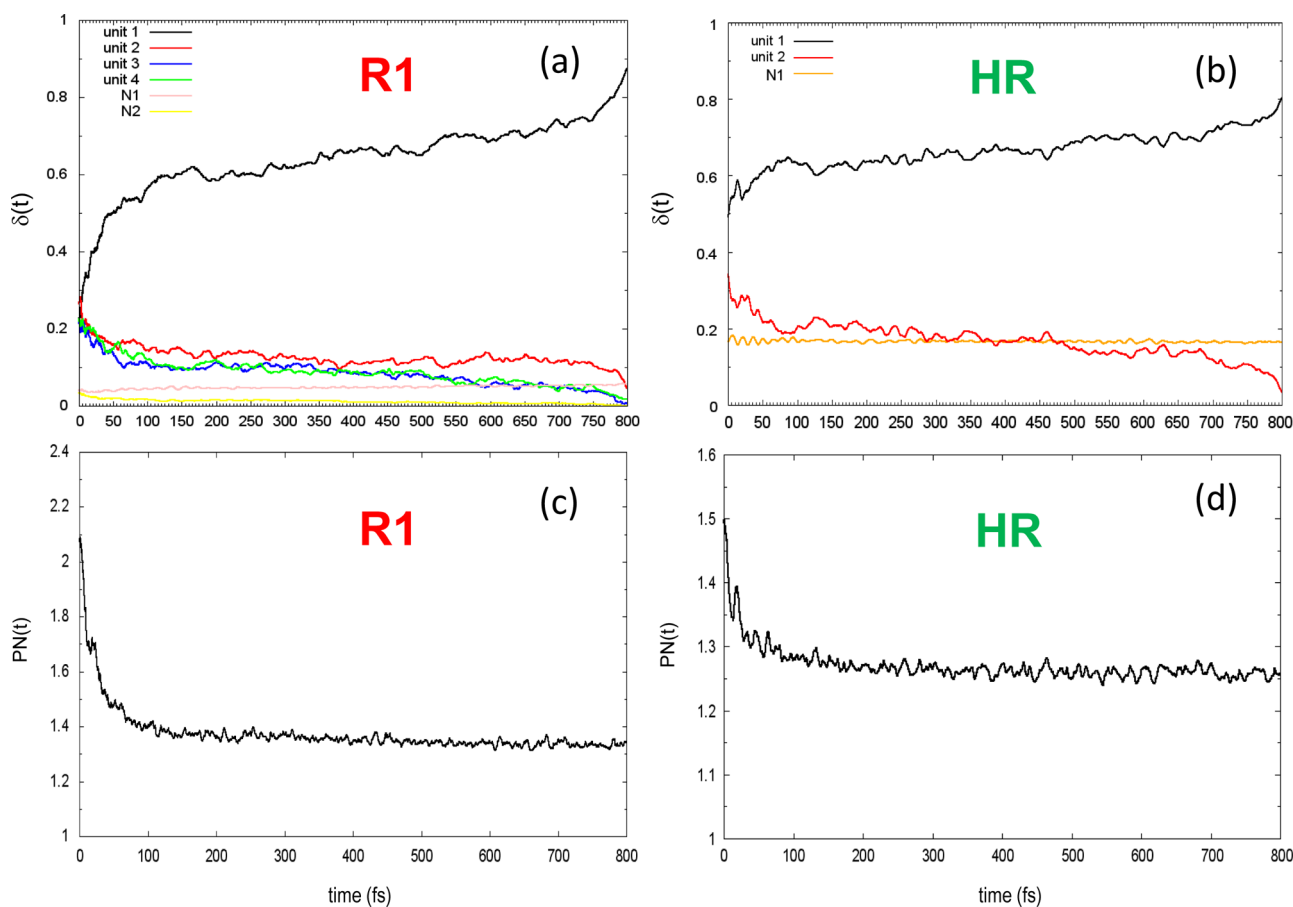
Figure 2. Evolution of the average fraction of transition density (TD), $\delta(t)$, localized in each unit for R1 (a) and HR (b). TD matrices between ground (0) and excited (α) states, $(\rho^{0\alpha})_{nm}$, are calculated using the CEO method[45,46] within the CIS approximation such that $\sum_{n,m}(\rho^{0\alpha})^2_{nm} = 1$.[40] Summing the contributions from each atom (index A) gives $\delta^\alpha_X = (\rho^{0\alpha})^2_X = \sum_{n_A m_A}(\rho^{0\alpha})^2_{n_A m_A}$, the fraction of TD localized on each unit X. The corresponding change in the average participation number, $PN(t)$, shows the extent of (de)localization of the excitation for R1 (c) and HR (d). The participation number per unit X is defined as $PN = [\sum_X (\delta^\alpha_X)^2]^{-1}$ where $1 \leq PN \leq 4$ for R1 and $1 \leq PN \leq 2$ for HR. $PN \approx 1$ indicates TD localization to a single unit, and $PN \approx 4$ and 2 represents delocalization over all units of R1 and HR, respectively.

(toluene) spectra[22] which revealed very similar absorption for the two compounds with peaks at 375 and 320 nm (R1) and 383 and 306 nm (HR). Our computed spectra show absorption peaks at 373 and 302 nm (R1) and 384 and 292 nm (HR). In both R1 and HR, the four lowest-energy excited states, S_1–S_4, give rise to the lowest-energy peak, and their individual contributions to the equilibrated absorption spectra are provided in Figure S1. In R1, S_1–S_4 give relatively equal contributions, whereas the dominant contribution in HR arises only from S_1 and S_2. It is interesting to consider the equilibrium TD localization of the relevant excited states S_1–S_4, computed as vertical transitions, depicted in Figure S2. At the equilibrium geometry, S_1–S_4 are delocalized over all four units in R1. However, in HR, S_1 and S_2 are delocalized while S_3 and S_4 are localized on opposite units. Therefore, delocalized excitonic states are primarily responsible for the lowest-energy absorption peak in both compounds.

We first consider the energy transfer, as revealed through changes in the spatial localization of the electronic TD, among the four units comprising R1 and the two units in HR following excitation to the lowest-energy absorption peak. In each trajectory, unit 1 is assigned as the unit with the largest TD fraction, $\delta_X(t)$, at the end of dynamics. The other units are assigned clockwise from unit 1, and the pyridine links are denoted as N. The evolution of the fraction of TD localized in

each unit of R1 can be seen in Figure 2a. After the initial photoexcitation of R1, the probability of finding electronic TD in each of the units is equal because the initial excitation can be generated on either the top or bottom half of R1. Thus, the initial delocalization of the equilibrium geometry observed in Figure S2 is destroyed by thermally induced geometry fluctuations. This is confirmed by the evolution of the participation number in R1 shown in Figure 2c, where the average initial value of $PN(t)$ is 2.1, indicating that the initial excitation in R1 is delocalized over the two units comprising either the top or bottom half of the macrocycle (units 1 and 2 or units 3 and 4). The distribution of the initial participation number provided in Figure S3 confirms the most probable initial contribution ranging from 1.8 to 2.2 units. Note that the pyridine linkages do not play a significant role in the initial TD localization in R1 (Figure 2a).

Meanwhile, the initial excitation in HR is somewhat localized in unit 1 (Figure 2b) with varying levels of delocalization over the two units, giving unit 2 a substantial initial fraction of TD where an average of 1.5 units participate in the initial delocalization according to the evolution of the participation number in Figure 2d. The distribution of the initial participation number in HR (Figure S3) confirms that both localized as well as delocalized excitations are initially formed. We find that in ~16% of trajectories, the initial excitation in HR

is completely delocalized, while in ∼22% of trajectories there is a strong localization in unit 1. The remaining trajectories showed varying degrees of initial delocalization, indicating that the pyridine meta linkage does not completely inhibit delocalization. Within both systems, however, there is a rapid redistribution of excitation energy to unit 1 within 200 fs, as evidenced by the rise in the TD fraction localized within unit 1 and the corresponding decrease in the TD fraction localized in all other units (Figure 2a,b). At the same time, the participation number decreases in both systems to ∼1.3 (Figure 2c,d). The pyridine linkage N1 retains a significant fraction of the final TD in HR, and in R1 both the N1 linkage and unit 2 contain a small fraction of the final TD, causing the final participation number to be greater than the expected value of 1 in both systems.

The rate of energy transfer was calculated by fitting the increase of TD in unit 1 from the curves in Figure 2a,b to a biexponential function. Our fits (shown in Figure S4) consist of fast and slow time components corresponding to τ_1 and τ_2, respectively. The fitting parameters are provided in Table 1.

Table 1. Biexponential Fitting Parameters for the Average Fraction of Transition Density and Accumulated Flux[a]

	A_1	τ_1 (fs)	A_2	τ_2 (fs)	y_0
HR TD unit 1	−0.124	29.1	0.033	469.3	0.665
R1 TD unit 1	−0.341	38.5	0.030	387.2	0.556
R1 flux 2 → 1	−0.077	34.3	0.018	485.4	0.074
R1 flux 3 → 1	−0.129	33.8	0.004	257.9	0.123
R1 flux 4 → 1	−0.108	42.0	0.039	827.1	0.068

[a]The fitting function is given by $f(t) = A_1 \exp(-t/\tau_1) + A_2 \exp(t/\tau_2) + y_0$.

The fast component, τ_1, makes the dominant contribution, A_1, and is therefore the focus of our analysis, revealing different time scales for R1 and HR. A time scale of 38.5 ± 0.3 fs was found for R1, while HR exhibits a faster time scale of 29.1 ± 0.7 fs. In HR, an initially delocalized excitation will undergo rapid energy transfer to become localized in unit 1. Meanwhile in R1, regardless of whether the excitation is initially generated on the top or bottom half of the ring, the final localization is always in the upper half in unit 1. Therefore, in R1, the relaxation consists of simultaneous energy-transfer pathways. This can be seen by tracking the angle, Θ, between the final TD moment at the end of the simulated dynamics and the TD moment at time t, shown in Scheme 1a. The angles for R1 and HR are depicted in Scheme 1b−d. The contour plot of R1 in Scheme 1b shows the fast decay of initial TD localization in units 3 and 4 within the first 200 fs as the excitation becomes localized in unit 1. The TD localization in unit 2 persists slightly longer as is also seen in the slightly larger fraction of TD retained in unit 2 in Figure 2a. Within 100 fs, however, the majority of TD is transferred to unit 1. The different color scale in Scheme 1c,d reveals the presence of intermediate angles in R1 and HR indicating delocalization; for example, the signal at 30° corresponds to a delocalization between units 1 and 2 caused by electronic coupling. Interestingly, there is no trace of any persistent coupling between the symmetric units 3 and 4 in R1, which would appear at 210°, or between any other units. Couplings between units are also reflected in the initial participation numbers (Figure 2c,d), indicating an initial delocalization involving more than 2 and 1 units for R1 and

HR, respectively. Therefore, interference of interchromophoric energy-transfer pathways is expected.

The energy-transfer flow between each unit in R1 is revealed from the accumulated TD flux in Figure 3. The top left panel shows the accumulated TD in unit 1 received from all other units. All of the units make only positive contributions to unit 1; therefore, unit 1 behaves only as an acceptor and never as a donor. Meanwhile, units 2, 3, and 4 *do not interchange TD among each other*, rather they only donate TD directly to unit 1 indicated by the negative flux for the $1 − X$ component where X is the donor unit. From the flow analysis, the energy-transfer time scale in R1 can be decomposed into contributions from each pathway (see fitting parameters in Table 1). Flow from unit 2 to 1 and unit 3 to 1 occurs on the same time scale with values of 34.3 ± 0.6 fs and 33.8 ± 0.2 fs, respectively, while transfer from unit 4 to 1 is slower at 42.0 ± 0.5 fs. Interestingly, the presence of the additional chromophores in R1 compared to HR results in a slower transfer between units 2 and 1 in R1 compared to the time scale of 29.1 ± 0.7 fs computed in HR, where flow can occur only from unit 2 to 1. Even though the donor units in R1 do not exchange TD among each other, the pathways interfere to slow the overall energy-transfer rate.

Finally, the time-resolved fluorescence anisotropy can also be used to follow changes in exciton localization. To verify the energy-transfer dynamics of the TD analysis, fluorescence anisotropy decay signals were computed from the NA-ESMD simulations as described in eqs 3−7. A nonzero value of C_∞ is indicative of the stationary orientational anisotropy in the system. It can be interpreted as an order parameter and can be estimated, for example, within the diffusion-in-the-cone model.[35] Evidently, the simulated fluorescence anisotropy curves shown in Figure 4 are in very good agreement with previously reported experimental results.[22] It is crucial to note that when comparing calculation and measurement, only the difference in $r(t)$ between the two compounds is of interest, not the overall absolute magnitudes, which can be affected by experimental offsets. With the same parameter set, the simulations reproduce the difference in $r(t)$ between the two compounds. Without the interference effect, $r(t)$ for R1 would be even lower and would approach an initial value of 0.1, becoming independent of time, as expected for a two-dimensional chromophore. This effect has been observed in larger conjugated macrocycles.[36]

Understanding and analysis of energy-transfer processes governed by the intricate interplay between chemical structure, conformational disorder, electron−phonon coupling, and excitonic effects is essential for many technologies based on organic semiconductor materials. Numerous previous experimental and theoretical efforts elucidated complex excited-state dynamics commensurate with energy transduction in linear, circular, and branched molecular architectures, which goes beyond simple models like the Förster framework. Atomistic simulations of such dynamics beyond the Born−Oppenheimer limit provide copious details of the underlying photophysics and establish structure−property relationships.

Here, we have performed NA-ESMD simulations of the nonradiative relaxation and energy-transfer dynamics in a π-conjugated phenylene−ethynylene macrocycle and corresponding half ring and used a new transition density flux approach to analyze our results. It is important to note that interactions between units that do not lead to a final average unidirectional energy transfer cannot be observed with our method, representing a limitation of the transition density flux analysis.

Scheme 1. (a) Angle, Θ, between Transition Density Moments at time t (left) and at the End of Dynamics (right); (b) Contour Density Plot of $\Theta(t)$ on a Logarithmic Scale for R1 (up to t = 600 fs) Where Angles 0°, 60°, 180°, and 240° Correspond to Units 1, 2, 3, and 4, respectively; (c) Rescaled Contour Density Plot of $\Theta(t)$ for R1 (up to t = 800 fs) Showing Intermediate Angles (d) Contour Density Plot of $\Theta(t)$ for HR with 0° and 60° Corresponding to Units 1 and 2, Respectively
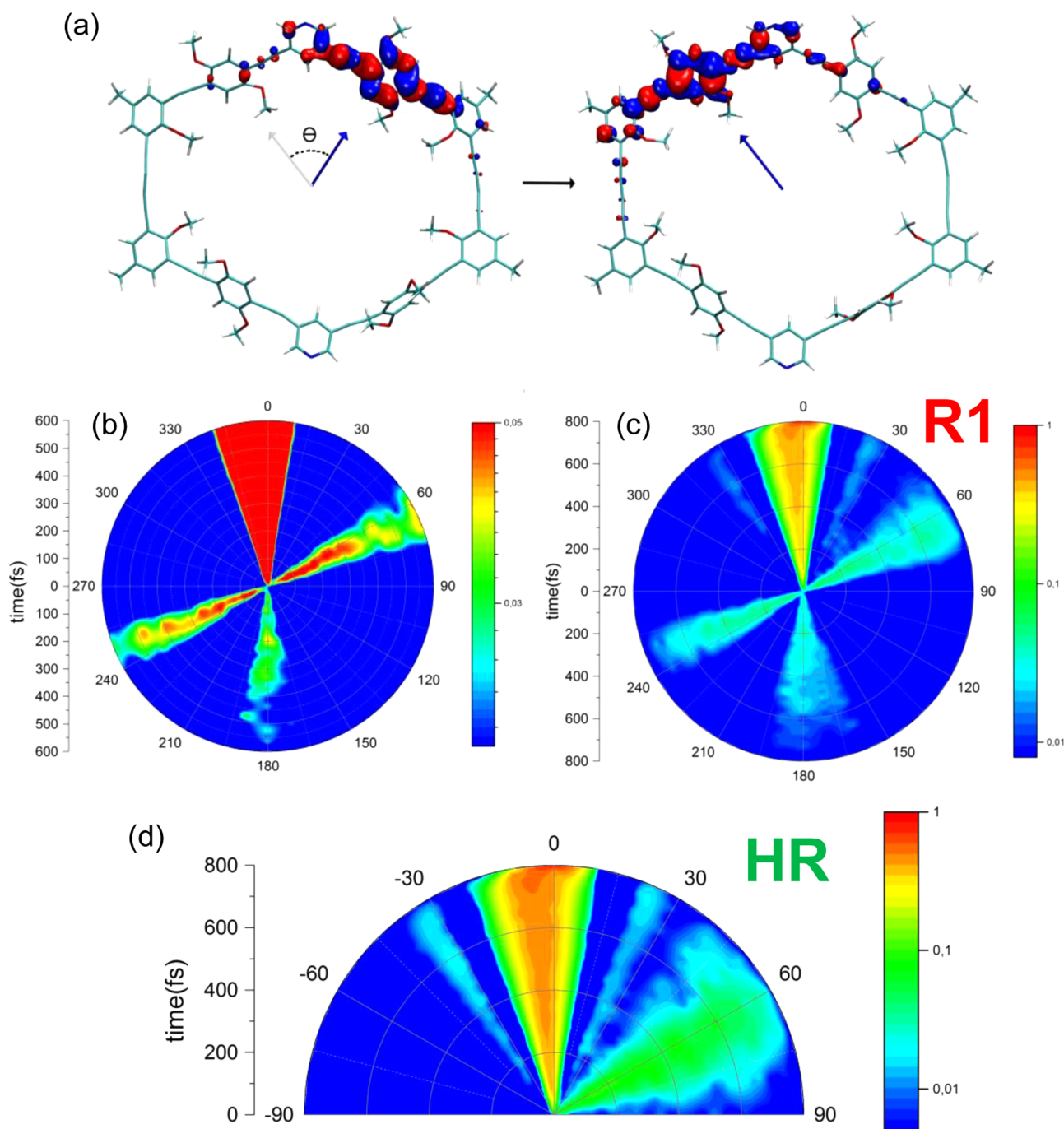

In both systems, an initially delocalized excitation undergoes ultrafast energy transfer to a single chromophore unit, representing a localized emissive state. In contrast to CPPs, where spatially localized excitons can span several phenyl rings,[19] the localization in the phenylene−ethynylene macrocycle involves only a single unit. The rapid localization occurs on a time scale of 29.1 ± 0.7 fs in the half-ring system and is unexpectedly slowed to 38.5 ± 0.3 fs in the macrocycle. In the half ring, transition density flows only from unit 2 to 1. In the macrocycle, unique pathways consist of changing the localization from the bottom of the ring (units 3 and 4) directly to

unit 1. At the same time, a pathway analogous to that observed in the half ring also exists in the macrocycle where transition density flows from unit 2 directly to unit 1. There is no energy transfer between the other units (units 2, 3, and 4) comprising the macrocycle, instead they act only as donors with unit 1 as the acceptor. Despite this, the presence of additional units in the macrocycle causes the overall energy transfer to become slower compared to that of the half ring, even though the energy-transfer pathways from unit 2 to 1 are seemingly identical on both halves of the macrocycle. Therefore, the longer time scale observed in the fluorescence anisotropy decay
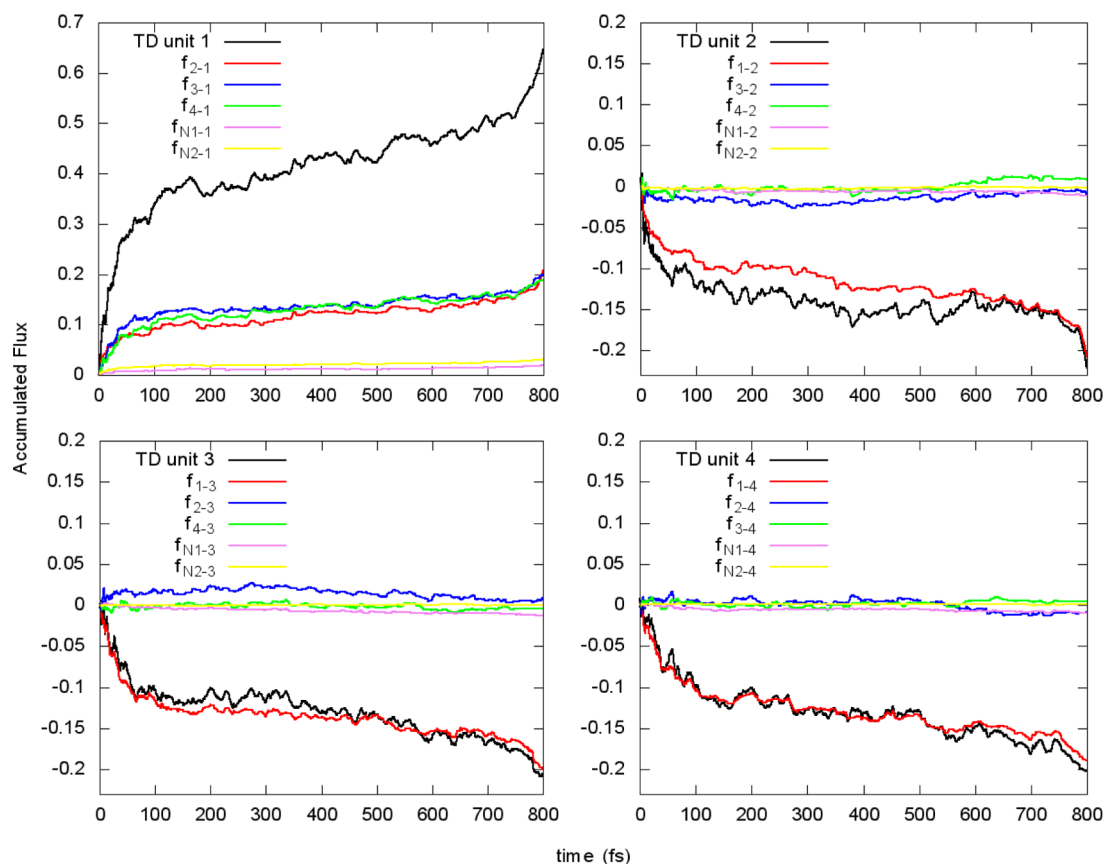
Figure 3. Accumulated flux for each unit in R1 computed using the transition density flux analysis. The contributions from the N linkages are negligible. Exponential fits (not shown) of the curves for units $X - 1$ (for $X = 2, 3, 4$) in the plot of TD unit 1 (upper left) are used to determine the role of individual pathways in the overall energy-transfer rate.
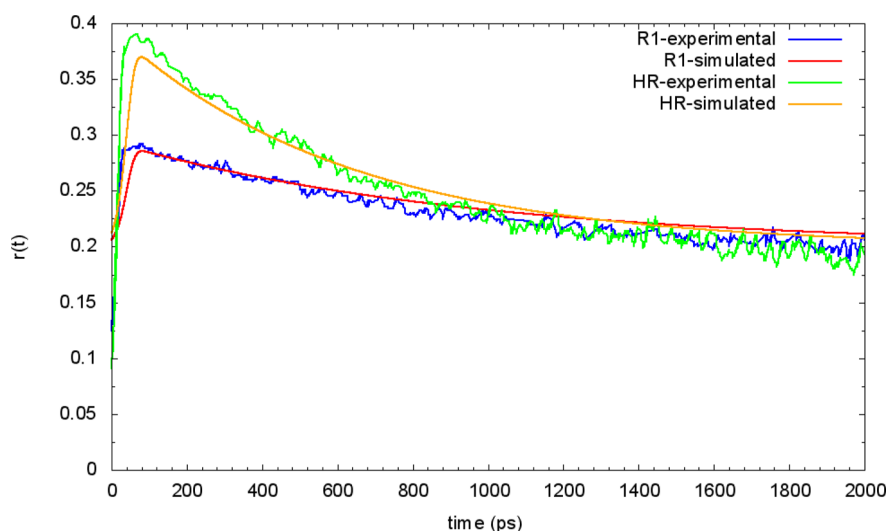
Figure 4. Simulated and experimental fluorescence anisotropy signals for HR and R1. The following parameters were used to fit to experimental curves:[22] $t_{sim} = 800$ fs; $t_{ini} = 20$ ps; $\tau = 1$ ns; 2FWHM = 50 ps (according to the experimental time resolution); the rotational diffusion coefficients $\tau_R = 954$ ps for R1 and $\tau_R = 620$ ps for HR; and $C_\infty = 0.2$.

of the macrocycle compared to the half-ring results from multiple interfering energy-transfer pathways.

In CPPs, self-trapping is expected to be more prominent in larger rings that can easily form regions of local planarity. In contrast, energy transfer in the present system does not depend on planarization in the excited state, and we expect that interference phenomena should become less significant as the

size of the macrocycle increases and energy transfer becomes more Förster-like. Indeed, larger conjugated phenylene–ethynylene macrocycles with a diameter of 7 nm have been shown to exhibit ultrafast depolarization to the expected value of 0.1 within the experimental time resolution,[36] implying that interference effects play a lesser role in these larger systems. Finally, it is also interesting to note the similarity of the present

discussion on the flow of excitation energy, and the interference of flow pathways, with the interference of electronic conduction pathways in molecular junctions.[37] It is quite intriguing to contrast the respective foundations of excitonics and electronics—the Born−Oppenheimer approximation and Kirchhoff's law—and their respective breakdown due to quantum interference phenomena. Such detailed comparison of energy-transfer dynamics from a computational perspective allows for direct parallels of dynamics in quasi-linear oligomers (frequently exploited in artificial light-harvesters such as dendrimers) and near-circular structure (the geometry found in natural photosynthetic complexes). Insights obtained provide useful guidelines for ongoing time-resolved spectroscopic investigations in a variety of conjugated materials, whereas the transition density flux approach is expected to be a convenient analysis tool in future theoretical studies of other systems.

■ COMPUTATIONAL METHODS

NA-ESMD Methodology and Simulation Details. The NA-ESMD framework allows the nonradiative relaxation through many electronic excited states to be simulated in large molecular systems. A set of independent classical nuclear trajectories is propagated on a single adiabatic excited-state potential energy surface (PES) via constant-temperature Langevin dynamics.[38,39] Transitions among excited states are incorporated through the FSSH algorithm[33] in which the electronic wave function evolution is described by excited-state energies, gradients, and nonadiabatic couplings evaluated "on the fly" with analytical techniques.[31,40−44] The Collective Electronic Oscillator (CEO) approach[45,46] is used to compute electronic excited states at the configuration interaction singles (CIS) level of theory and has been implemented with the semiempirical PM3 Hamiltonian.[47,48] This method has been successful in modeling nonadiabatic dynamics of excitonic states in organic conjugated materials.[45,49−53] A detailed description of the NA-ESMD methodology and limitations can be found elsewhere.[31,32,54−57] Initial geometries and momenta were sampled from ground-state dynamics for R1 (80 ps; 1000 snapshots) and HR (100 ps; 800 snapshots) computed using a Langevin thermostat (300 K) with a friction coefficient of 20 ps^{-1}. The initial excited state was selected using a Franck−Condon window defined as $g_\alpha(r,R) = (f_\alpha/\Omega_\alpha^2) \exp[-T^2 E_{ex} - \Omega_\alpha^2]$ with temporal line shape $f(t) = \exp(-t^2/2T^2)$, where $T = 42.5$ fs corresponds to a full width at half-maximum (FWHM) of 100 fs. f_α and Ω_α are the normalized oscillator strength and the frequency of state α, and E_{ex} is the excitation energy. The NA-ESMD trajectories were propagated for 800 fs with a classical time step of $\Delta t = 0.1$ fs at 300 K using a friction coefficient of 20 ps^{-1} where states $S_1 - S_4$ have been considered. A total of 401 (R1) and 301 (HR) converged trajectories were obtained.

Transition Density Flux. The transition density flux analysis described here is adapted from the SMF method, developed by Soler et al., applied to the vibrational energy flow in polyatomic molecules.[34] The change in the TD fraction localized on unit X during time step Δt is given by $\Delta\delta_X(t) = \delta_X(t + \Delta t) - \delta_X(t)$ (the superindex indicating the PES for the NA-ESMD propagation has been omitted). A detailed description of TD interchange between units is contained in the flow matrix $\mathbf{F}(t)$ with diagonal elements of zero and off-diagonal elements $f_{XY}(t)$ containing the amount of TD transferred between units X and Y in the time interval Δt, fulfilling the requirement $f_{XY}(t) = -f_{YX}(t)$. Considering that $f_{XY}(t) > 0$ represents an effective

transfer of TD from unit X to Y, we can write $\Delta\delta_X(t) = \sum_Y^4 f_{YX}(t)$ for R1. Imposing the minimum flow criterion, which assumes that the amount of TD exchanged by unit X during Δt is a minimum, allows units to be classified as TD donors (D) if $\Delta\delta_X(t) < 0$ or TD acceptors (A) if $\Delta\delta_X(t) > 0$. The SMF method assumes that TD flows only from D to A such that the total TD exchanged among units during Δt is

$$\Delta\delta_{totoal}(t) = \sum_{X \in D} |\Delta\delta_X(t)| = \sum_{Y \in A} |\Delta\delta_Y(t)| \tag{1}$$

In this way, the elements $f_{XY}(t)$ can be computed as

$$f_{XY}(t) = -f_{YX}(t)$$
$$= \begin{cases} \dfrac{|\Delta\delta_X(t)|\Delta\delta_Y(t)}{\Delta\delta_{total}(t)} & X \in D, Y \in A \\[2mm] 0 & X, Y \in D \text{ or } X, Y \in A \end{cases} \tag{2}$$

A detailed derivation of eq 2 can be found in the Supporting Information and elsewhere.[34]

Fluorescence Anisotropy. The fluorescence anisotropy is determined by the time correlation function of the absorption dipole moment of the chromophore at time zero, $\vec{\mu}_A(t = 0)$, and its emission dipole moment at time t, $\vec{\mu}_E(t)$[35]

$$C(t) = \frac{2}{5}\langle P_2\{\vec{\mu}_A(0)\cdot\vec{\mu}_E(t)\}\rangle \tag{3}$$

where $P_2(x) = \frac{1}{2}(3x^2 - 1)$ is the second-order Legendre polynomial and x is the cosine of the angle between the excitation and emission dipole moments; the angular brackets indicate the average over all NA-ESMD trajectories. Equation 3 refers to an ideal fluorescence signal excited by an infinitely short laser pulse. To account for a more realistic pulse of finite duration, the fluorescence anisotropy, $r(t)$, can be computed via the convolution of $C(t)$ with the Gaussian pulse-shape function:

$$r(t) = \frac{\int_0^\infty dt' N(t - t' - t_{ini})\, e^{-t'/\tau} C(t')}{\int_0^\infty dt' N(t - t' - t_{ini}) e^{-t'/\tau}} \tag{4}$$

$$N(t - t_{ini}) = \exp[-(t - t_{ini})^2/\text{FWHM}^2] \tag{5}$$

Here, t_{ini} is the arrival time of the excitation pulse and τ is the fluorescence lifetime. The correlation function, $C(t)$, is simulated in the present work on the time scale of $t_{sim} = 800$ fs and is referred to as $C_{sim}(t)$ hereafter. $C_{sim}(t)$, shown in Figure S5, shows a fast decay within the first 50 fs and further exhibits irregular small-amplitude oscillations around the quasi-stationary value $C_{sim}(t_{sim})$. On the other hand, a characteristic time scale of the anisotropy evolution detected in ref 22, t_{exp}, spans a few nanoseconds and is determined by a slow reorientation governed by the rotational diffusion coefficient, D. Hence, the correlation function in eq 3 can be expressed in terms of $C_{sim}(t)$ as

$$C(t) = \tilde{C}_{sim}(t) + C_\infty \tag{6}$$

where

$$\tilde{C}_{sim}(t) = \begin{cases} C_{sim}(t)e^{-t/\tau_R} & t \leq t_{sim} \\ C_{sim}(t_{sim})e^{-t/\tau_R} & t > t_{sim} \end{cases} \tag{7}$$

Here, $\tau_R = (6D^{-1})$ is the rotational diffusion relaxation time and C_∞ is a stationary value of the correlation function, which accounts for a possible incomplete orientational relaxation during the time interval t_{exp}.[35]

■ ASSOCIATED CONTENT

Ⓢ Supporting Information

The Supporting Information is available free of charge on the ACS Publications website at DOI: 10.1021/acs.jpclett.6b02236.

Figures of simulated absorption spectra with contributions from individual states, equilibrium electronic transition density localization, histograms of participation number for initial configurations, biexponential fit of transition density, and the simulated time correlation function $C_{sim}(t)$; further details on the derivation of transition density flux method (PDF)

■ AUTHOR INFORMATION

Corresponding Authors

*E-mail: serg@lanl.gov.
*E-mail: sfalberti@gmail.com.

ORCID Ⓘ

Tammie Nelson: 0000-0002-3173-5291

Notes

The authors declare no competing financial interest.

■ ACKNOWLEDGMENTS

■ REFERENCES

(1) Wolfer, P.; Armin, A.; Pivrikas, A.; Velusamy, M.; Burn, P. L.; Meredith, P. Solution Structure: Defining Polymer Film Morphology and Optoelectronic Device Performance. *J. Mater. Chem. C* **2014**, *2*, 71−77.

(2) Schmidt-Hansberg, B.; Sanyal, M.; Klein, M. F.; Pfaff, M.; Schnabel, N.; Jaiser, S.; Vorobiev, A.; Muller, E.; Colsmann, A.; Scharfer, P.; et al. Moving Through the Phase Diagram: Morphology Formation in Solution Cast Polymer-Fullerene Blend Films for Organic Solar Cells. *ACS Nano* **2011**, *5*, 8579−8590.

(3) Nie, W.; Gupta, G.; Crone, B. K.; Liu, F.; Smith, D. L.; Ruden, P. P.; Kuo, C.; Tsai, H.; Wang, H.; Li, H.; et al. Interface Design Principles for High-Performance Organic Semiconductor Devices. *Adv. Sci.* **2015**, *2*, 1500024.

(4) Nguyen, T.-Q.; Schwartz, B. J. Ionomeric Control of Interchain Interactions, Morphology, and the Electronic Properties of Conjugated Polymer Solutions and Films. *J. Chem. Phys.* **2002**, *116*, 8198.

(5) Ondarse-Alvarez, D.; Oldani, N.; Tretiak, S.; Fernandez-Alberti, S. Computational study of photoexcited dynamics in bichromophoric cross-shaped oligofluorene. *J. Phys. Chem. A* **2014**, *118*, 10742−10753.

(6) Tretiak, S.; Zhang, W. M.; Chernyak, V.; Mukamel, S. Excitonic couplings and electronic coherence in bridged naphthalene dimers. *Proc. Natl. Acad. Sci. U. S. A.* **1999**, *96*, 13003−13008.

(7) Alfonso Hernandez, L.; Nelson, T.; Tretiak, S.; Fernandez-Alberti, S. Photoexcited Energy Transfer in a Weakly Coupled Dimer. *J. Phys. Chem. B* **2015**, *119*, 7242−7252.

(8) Bredas, J.-L.; Beljonne, D.; Coropceanu, V.; Cornil, J. Charge-Transfer and Energy-Transfer Processes in π-Conjugated Oligomers and Polymers: A Molecular Picture. *Chem. Rev.* **2004**, *104*, 4971−5003.

(9) Lin, H.-C.; Jin, B.-Y. Charge-Transfer Interactions in Organic Functional Materials. *Materials* **2010**, *3*, 4214−4251.

(10) Brown, P. J.; Thomas, D. S.; Kohler, A.; Wilson, J. S.; Kim, J.-S.; Ramsdale, C. M.; Sirringhaus, H.; Friend, R. H. Effect of Interchain Interactions on the Absorption and Emission of Poly(3-Hexylthiophene). *Phys. Rev. B: Condens. Matter Mater. Phys.* **2003**, *67*, 064203.

(11) Sundstrom, V.; Pullerits, T.; van Grondelle, R. Photosynthetic Light-Harvesting: Reconciling Dynamics and Structure of Purple Bacterial LH2 Reveals Function of Photosynthetic Unit. *J. Phys. Chem. B* **1999**, *103*, 2327−2346.

(12) Ye, J.; Sun, K.; Zhao, Y.; Yu, Y.; Lee, C. K.; Cao, J. Excitonic Energy Transfer in Light-Harvesting Complexes in Purple Bacteria. *J. Chem. Phys.* **2012**, *136*, 245104.

(13) Ricci, M.; Bradforth, S. E.; Jimenez, R.; Fleming, G. R. Internal Conversion and Energy Transfer Dynamics of Spheroidene in Solution and in the LH-1 and LH-2 Light-Harvesting Complexes. *Chem. Phys. Lett.* **1996**, *259*, 381−390.

(14) Ostroumov, E. E.; Mulvaney, R. M.; Anna, J. M.; Cogdell, R. J.; Scholes, G. D. Energy Transfer Pathways in Light-Harvesting Complexes of Purple Bacteria as Revealed by Global Kinetic Analysis of Two-Dimensional Transient Spectra. *J. Phys. Chem. B* **2013**, *117*, 11349−11362.

(15) Bolinger, J. C.; Traub, M. C.; Brazard, J.; Adachi, T.; Barbara, P. F.; Vanden Bout, D. A. Conformation and Energy Transfer in Single Conjugated Polymers. *Acc. Chem. Res.* **2012**, *45*, 1992−2001.

(16) Van Averbeke, B.; Beljonne, D. Conformational Effects on Excitation Transport along Conjugated Polymer Chains. *J. Phys. Chem. A* **2009**, *113*, 2677−2682.

(17) Kim, T.-W.; Kim, W.; Park, K. H.; Kim, P.; Cho, J.-W.; Shimizu, H.; Iyoda, M.; Kim, D. Chain-Length-Dependent Exciton Dynamics in Linear Oligothiophenes Probed Using Ensemble and Single-Molecule Spectroscopy. *J. Phys. Chem. Lett.* **2016**, *7*, 452−458.

(18) Nelson, T.; Fernandez-Alberti, S.; Roitberg, A. E.; Tretiak, S. Conformational Disorder in Energy Transfer: Beyond Förster Theory. *Phys. Chem. Chem. Phys.* **2013**, *15*, 9245−9256.

(19) Adamska, L.; Nayyar, I.; Chen, H.; Swan, A. K.; Oldani, N.; Fernandez-Alberti, S.; Golder, M. R.; Jasti, R.; Doorn, S. K.; Tretiak, S. Self-Trapping of Excitons, Violation of Condon Approximation, and Efficient Fluorescence in Conjugated Cycloparaphenylenes. *Nano Lett.* **2014**, *14*, 6539−6546.

(20) Becker, K.; Da Como, E.; Feldmann, J.; Scheliga, F.; Thorn Csányi, E.; Tretiak, S.; Lupton, J. M. How Chromophore Shape Determines the Spectroscopy of Phenylene-Vinylenes: Origin of Spectral Broadening in the Absence of Aggregation. *J. Phys. Chem. B* **2008**, *112*, 4859−4864.

(21) Johnson, J. M.; Chen, R.; Chen, X.; Moskun, A. C.; Zhang, X.; Hogen-Esch, T. E.; Bradforth, S. E. Investigation of Macrocyclic Polymers as Artificial Light Harvesters: Subpicosecond Energy Transfer in Poly(9,9-dimethyl-2-vinylfluorene). *J. Phys. Chem. B* **2008**, *112*, 16367−16381.

(22) Becker, K.; Fritzsche, M.; Hoger, S.; Lupton, J. M. Phenylene−Ethynylene Macrocycles as Model Systems of Interchromophoric Interactions in π-Conjugated Macromolecules. *J. Phys. Chem. B* **2008**, *112*, 4849−4853.

(23) Schlosser, F.; Sung, J.; Kim, P.; Kim, D.; Wurthner, F. Excitation Energy Migration in Covalently Linked Perylene Bisimide Macrocycles. *Chem. Sci.* **2012**, *3*, 2778−2785.

(24) Varnavski, O.; Bauerle, P.; Goodson, T., III Strong Coupling in Macrocyclic Thiophene Investigated by Time-Resolved Two-Photon Excited Fluorescence. *Opt. Lett.* **2007**, *32*, 3083−3085.

(25) Yong, C.-K.; Parkinson, P.; Kondratuk, D.; Chen, W.-H.; Stannard, A.; Summerfield, A.; Sprafke, J.; O'Sullivan, M.; Beton, P.; Anderson, H.; et al. Ultrafast Delocalization of Excitation in Synthetic Light-Harvesting Nanorings. *Chem. Sci.* **2015**, *6*, 181−189.

(26) Camacho, C.; Niehaus, T.; Itami, K.; Irle, S. Origin of the Size-Dependent Fluorescence Blueshift in [n]Cycloparaphenylenes. *Chem. Sci.* **2013**, *4*, 187−195.

(27) Marcus, M.; Coonjobeeharry, J.; Barford, W. Theory of Optical Transitions in π-Conjugated Macrocycles. *J. Chem. Phys.* **2016**, *144*, 154102.

(28) Parkinson, P.; Kondratuk, D. V.; Menelaou, C.; Gong, J. Q.; Anderson, H. L.; Herz, L. M. Chromophores in Molecular Nanorings: When Is a Ring a Ring? *J. Phys. Chem. Lett.* **2014**, *5*, 4356−4361.

(29) Nishihara, T.; Segawa, Y.; Itami, K.; Kanemitsu, Y. Exciton Recombination Dynamics in Nanoring Cycloparaphenylenes. *Chem. Sci.* **2014**, *5*, 2293−2296.

(30) Nishihara, T.; Segawa, Y.; Itami, K.; Kanemitsu, Y. Excited States in Cycloparaphenylenes: Dependence of Optical Properties on Ring Length. *J. Phys. Chem. Lett.* **2012**, *3*, 3125−3128.

(31) Nelson, T.; Fernandez-Alberti, S.; Chernyak, V.; Roitberg, A. E.; Tretiak, S. Nonadiabatic Excited-State Molecular Dynamics Modeling of Photoinduced Dynamics in Conjugated Molecules. *J. Phys. Chem. B* **2011**, *115*, 5402−5414.

(32) Nelson, T.; Fernandez-Alberti, S.; Roitberg, A. E.; Tretiak, S. Nonadiabatic Excited-State Molecular Dynamics: Modeling Photophysics in Organic Conjugated Materials. *Acc. Chem. Res.* **2014**, *47*, 1155−1164.

(33) Tully, J. Molecular Dynamics with Electronic Transitions. *J. Chem. Phys.* **1990**, *93*, 1061−1071.

(34) Soler, M. A.; Bastida, A.; Farag, M. H.; Zuniga, J.; Requena, A. A Method for Analyzing the Vibrational Energy Flow in Biomolecules in Solution. *J. Chem. Phys.* **2011**, *135*, 204106.

(35) Szabo, A. Theory of Fluorescence Depolarization in Macromolecules and Membranes. *J. Chem. Phys.* **1984**, *81*, 150−167.

(36) Thiessen, A.; Würsch, D.; Jester, S.-S.; Aggarwal, A. V.; Idelson, A.; Bange, S.; Vogelsang, J.; Höger, S.; Lupton, J. M. Exciton Localization in Extended π-Electron Systems: Comparison of Linear and Cyclic Structures. *J. Phys. Chem. B* **2015**, *119*, 9949−9958.

(37) Vazquez, H.; Skouta, R.; Schneebeli, S.; Kamenetska, M.; Breslow, R.; Venkataraman, L.; Hybertsen, M. S. Probing the Conductance Superposition Law in Single-Molecule Circuits with Parallel Paths. *Nat. Nanotechnol.* **2012**, *7*, 663−667.

(38) Paterlini, M.; Ferguson, D. Constant Temperature Simulations using the Langevin Equation with Velocity Verlet Integration. *Chem. Phys.* **1998**, *236*, 243−252.

(39) Attard, P. Statistical Mechanical Theory for Non-Equilibrium Systems. IX. Stochastic Molecular Dynamics. *J. Chem. Phys.* **2009**, *130*, 194113.

(40) Tretiak, S.; Isborn, C.; Niklasson, A.; Challacombe, M. Representation Independent Algorithms for Molecular Response Calculations in Time-Dependent Self-Consistent Field Theories. *J. Chem. Phys.* **2009**, *130*, 054111.

(41) Tretiak, S.; Chernyak, V.; Mukamel, S. Recursive Density-Matrix-Spectral-Moment Algorithm for Molecular Nonlinear Polarizabilities. *J. Chem. Phys.* **1996**, *105*, 8914−8928.

(42) Furche, F.; Ahlrichs, R. Adiabatic Time-Dependent Density Functional Methods for Excited State Properties. *J. Chem. Phys.* **2002**, *117*, 7433−7447.

(43) Send, R.; Furche, F. First-Order Nonadiabatic Couplings from Time-Dependent Hybrid Density Functional Response Theory: Consistent Formalism, Implementation, and Performance. *J. Chem. Phys.* **2010**, *132*, 044107.

(44) Tavernelli, I.; Curchod, B. F. E.; Laktionov, A.; Rothlisberger, U. Nonadiabatic Coupling Vectors for Excited States within Time-Dependent Density Functional Theory in the Tamm-Dancoff Approximation and Beyond. *J. Chem. Phys.* **2010**, *133*, 194104.

(45) Tretiak, S.; Chernyak, V.; Mukamel, S. Two-Dimensional Real-Space Analysis of Optical Excitations in Acceptor-Substituted Carotenoids. *J. Am. Chem. Soc.* **1997**, *119*, 11408−11419.

(46) Tretiak, S.; Chernyak, V.; Mukamel, S. Collective Electronic Oscillators for Nonlinear Optical Response of Conjugated Molecules. *Chem. Phys. Lett.* **1996**, *259*, 55−61.

(47) Stewart, J. J. P. Optimization of Parameters for Semiempirical Methods. I. Method. *J. Comput. Chem.* **1989**, *10*, 209−220.

(48) Stewart, J. J. P. Optimization of Parameters for Semiempirical Methods. II. Applications. *J. Comput. Chem.* **1989**, *10*, 221−264.

(49) Dreuw, A.; Head-Gordon, M. Single-Reference Ab Initio Methods for the Calculation of Excited States of Large Molecules. *Chem. Rev.* **2005**, *105*, 4009−4037.

(50) Bazan, G. C.; Oldham, W. J.; Lachicotte, R. J.; Tretiak, S.; Chernyak, V.; Mukamel, S. Stilbenoid Dimers: Dissection of a Paracyclophane Chromophore. *J. Am. Chem. Soc.* **1998**, *120*, 9188−9204.

(51) Tretiak, S.; Chernyak, V.; Mukamel, S. Excited Electronic States of Carotenoids: Time-Dependent Density-Matrix-Response Algorithm. *Int. J. Quantum Chem.* **1998**, *70*, 711−727.

(52) Tretiak, S.; Chernyak, V.; Mukamel, S. Chemical Bonding and Size Scaling of Nonlinear Polarizabilities of Conjugated Polymers. *Phys. Rev. Lett.* **1996**, *77*, 4656−4659.

(53) Tretiak, S.; Chernyak, V.; Mukamel, S. Localized Electronic Excitations in Phenylacetylene Dendrimers. *J. Phys. Chem. B* **1998**, *102*, 3310−3315.

(54) Nelson, T.; Fernandez-Alberti, S.; Chernyak, V.; Roitberg, A.; Tretiak, S. Nonadiabatic Excited-State Molecular Dynamics: Numerical Tests of Convergence and Parameters. *J. Chem. Phys.* **2012**, *136*, 054108.

(55) Fernandez-Alberti, S.; Roitberg, A.; Nelson, T.; Tretiak, S. Identification of Unavoided Crossings in Nonadiabatic Photoexcited Dynamics Involving Multiple Electronic States in Polyatomic Conjugated Molecules. *J. Chem. Phys.* **2012**, *137*, 014512.

(56) Nelson, T.; Fernandez-Alberti, S.; Roitberg, A. E.; Tretiak, S. Artifacts Due to Trivial Unavoided Crossings in the Modeling of Photoinduced Energy Transfer Dynamics in Extended Conjugated Molecules. *Chem. Phys. Lett.* **2013**, *590*, 208−213.

(57) Nelson, T.; Fernandez-Alberti, S.; Roitberg, A. E.; Tretiak, S. Nonadiabatic Excited-State Molecular Dynamics: Treatment of Electronic Decoherence. *J. Chem. Phys.* **2013**, *138*, 224111.

(58) Tretiak, S.; Mukamel, S. Density Matrix Analysis and Simulation of Electronic Excitations in Conjugated and Aggregated Molecules. *Chem. Rev.* **2002**, *102*, 3171−3212.